

# Propagation of misfit dislocations from AlN/Si interface into Si

Z. Liliental-Weber<sup>a,\*</sup>, R.L. Maltez<sup>b</sup>, J. Xie<sup>c</sup>, H. Morkoç<sup>c</sup>

<sup>a</sup> Materials Sciences Division, Lawrence Berkeley National Laboratory, MS 62/203, 1 Cyclotron Road, Berkeley, CA 94720, USA

<sup>b</sup> Instituto de Física, UFRGS, C.P. 15051, 91501-970 Porto Alegre-RS, Brazil

<sup>c</sup> Department of Electrical Engineering, Virginia Commonwealth University, Richmond, VA 23284, USA

## ARTICLE INFO

Available online 7 June 2008

### Keywords:

A1. TEM

A1. Structural perfection

A1. Propagation of misfit dislocations

B1. GaN/AlN/Si interfaces

## ABSTRACT

A substantial improvement of the structural quality of GaN/AlN grown on He implanted Si has been described. Many misfit dislocations were redirected from the Al/Si interface and propagated to the Si substrate due to the formation of He bubbles in the substrate. Growth temperature of GaN/AlN was chosen to be the annealing temperature necessary for He bubble formation. The dependence on the He fluence, distance of He bubbles from the Si surface and cleaning procedure of the Si before growth have been described. The structural perfection of the GaN/AlN layers was compared to the layers grown on un-implanted Si.

© 2008 Published by Elsevier B.V.

## 1. Introduction

Recently epitaxial growth of GaN on Si substrates has gained increasing interest, since such a system presents possibilities for novel integrated devices based on GaN and Si [1–3] and reduced cost. Such a system would provide the potential for utilizing the strength of GaN in conjunction with advanced Si technology for integrated device structures. However, the large misfit between GaN and Si (14% between *a*-axes), growth of a polar crystal on non-polar substrates and the difference in thermal expansion coefficients may lead to a high density of lattice defects and antiphase disorder as observed in GaAs grown on Si [4]. Due to a lack of native substrates for growth of GaN, this material always needs to be grown using foreign substrates such as Al<sub>2</sub>O<sub>3</sub> or SiC. Therefore, different approaches need to be applied, such as lateral overgrowth and pendeo-epitaxy, to reduce defect density in the epi-layer [5–10]. Reduction of strain at the interface always leads to a lower defect density. Earlier results show [11,12] that He implantation through a pseudomorphic Si–Ge layer into Si substrates and subsequent annealing at 800 °C lead to complete strain relaxation and defect-free Si–Ge layers in comparison with un-implanted samples. He bubbles were formed in the annealed implanted Si. A much denser arrangement of tangled misfit dislocations was found at the interface between the Si–Ge and implanted Si substrates in comparison with regularly distributed misfit dislocations in un-implanted Si, where only 50% relaxation was obtained upon annealing at 1100 °C. A model was proposed [11] for strain relaxation due to the formation of dislocation loops

in the vicinity of He bubbles that annihilate with threading dislocations at the temperature when the loops become glissile and can glide toward the SiGe interface. It was proposed that one side of the loop is pinned at the interface, where it forms a strain-relieving misfit segment. The other side is driven by the mismatch stress to the surface, where an atomic step is generated.

In the case of GaN, however, pseudomorphic growth on Si is impossible due to the lattice misfit being too large. However, the idea of He implantation [11,12] is interesting and we wanted to learn if using implantation into Si could reduce stress and lead to a decrease in the defect density in GaN. We have chosen a completely different procedure than that used for Si–Ge and implanted He into Si before growth using the growth temperature of GaN/AlN as the annealing temperature. We assumed that He bubbles formed below the Si surface and the stress around them would allow misfit dislocations to interact with these bubbles (or dislocation loops around them) and that segments of the threading dislocations would be redirected into the substrate instead of propagating into the GaN layer. In this case the implantation dose, distance of the He bubbles from the growth surface and the growth temperature had to be determined in order for the misfit dislocations formed at the AlN/Si interface to interact with these bubbles. According to our knowledge this procedure was applied for the first time. Therefore, all parameters have to be determined empirically. The experimental procedure will be described in the next section. Rutherford backscattering spectrometry (RBS) and transmission electron microscopy (TEM) were used to determine at which temperature the He bubbles were formed and how their presence influenced the structural perfection of the GaN. For comparison GaN/AlN layers were also grown on un-implanted Si substrates.

\* Corresponding author. Tel.: +1510 486 6276; fax: +1510 486 4995.

E-mail address: [z\\_liliental-weber@lbl.gov](mailto:z_liliental-weber@lbl.gov) (Z. Liliental-Weber).

## 2. Implantation conditions

Bare Si(111) samples were implanted with 15 and 30 keV of He ions up to fluences of 0.5, 1 and  $2 \times 10^{16} \text{ cm}^{-2}$ . The 30 keV implantation was used only up to the fluence of  $1 \times 10^{16} \text{ cm}^{-2}$ . In order to change the distance of the He bubbles from the Si surface, some samples with an additional 50 nm of  $\text{SiO}_2$  deposited on (111) Si sample were implanted with He at 15 keV and a fluence of  $1 \times 10^{16} \text{ cm}^{-2}$ . After implantation, the  $\text{SiO}_2$  cap layer was removed by etching in an  $\text{HF:H}_2\text{O}$  (1:2) solution, leaving the He profile shallower in comparison to the samples where bare Si was used. This alternative procedure was employed since an implantation energy lower than 15 keV was not available. In order to grow the  $\text{SiO}_2$  cap layer, Si was submitted to a controlled furnace annealing under a flux of high-purity dry  $\text{O}_2$ . All implantations were performed at room temperature using a 500 kV ion implanter. In order to detect the presence of He bubbles and their depth below the Si surface, implanted samples were subjected to rapid thermal annealing (RTA) for 120 s at different temperatures ranging from 350 to 1000 °C under  $\text{N}_2$  flux. All samples were analyzed by RBS, under random incidence and also aligned to the [111] sample direction (channeling normal to the surface). The measurements were carried out with a 1.2 MeV  $\text{He}^+$  beam produced by a 3 MV Tandem accelerator at Porto Alegre.

## 3. RBS/channeling studies

### 3.1. Short description of RBS/channeling methods

All samples were characterized by RBS aligned along the [111] Si crystallographic direction at which channeling can be obtained. Channeling is a special phenomenon observed in crystals, which allows the incoming beam of  $\alpha$  particles to penetrate in the interstitial positions and to be parallel to the low-index crystallographic directions of the sample [13]. In our RBS measurement a 1.2 MeV  $\text{He}^+$  beam impinged toward the sample surface and was collected by a detector placed at a fixed angular position. The signal generated in the detector was amplified and processed by a multichannel analyzer (MCA), where there is a linear relationship between the MCA channel number and  $\alpha$  particle energy. Particles backscattered from deeper in the sample will lose more energy due to their longer penetration depth and will produce counts at lower MCA channel numbers, representing lower energies. The final data have the form of a spectrum, as those shown in Figs. 1 and 2.

The sample is mounted on a goniometer with a precision better than  $0.1^\circ$ . When the beam is aligned with the low-index axial direction of a single crystal, the counts decrease to 2–5% compared to the value registered for a random atom distribution (a non-crystallographic direction, similar to that observed for an amorphous sample). Such a spectrum can be obtained by tilting the sample  $3\text{--}4^\circ$  from the aligned angular position, at which maximum counts can be obtained (see the non-aligned spectrum in Fig. 1).

### 3.2. Results from RBS/channeling measurements

The RBS/channeling measurements were performed on the implanted samples after annealing for 120 s (Figs. 1 and 2) in order to determine the best condition for He bubble formation in our samples. It has been observed earlier [14] that the presence of the over-pressurized bubbles results in a strong dechanneling of the incoming beam of  $\alpha$  particles at the depth of bubble formation. This can be a consequence of the stress generated by the bubbles

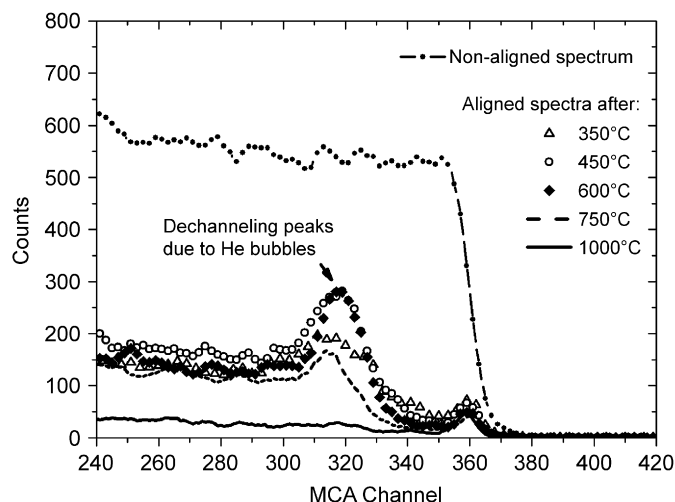


**Fig. 1.** Channeling measurements performed on the sample implanted with 15 keV of He ions, up to a fluence of  $2 \times 10^{16} \text{ He/cm}^2$ , after RTA annealing for 120 s at different temperatures: 350 °C (open triangles), 450 °C (open circles), 600 °C (full diamonds), 750 °C (dashed lines), 1000 °C (solid line). A non-aligned spectrum (uppermost, with dots) shows the maximum counts level for comparison.

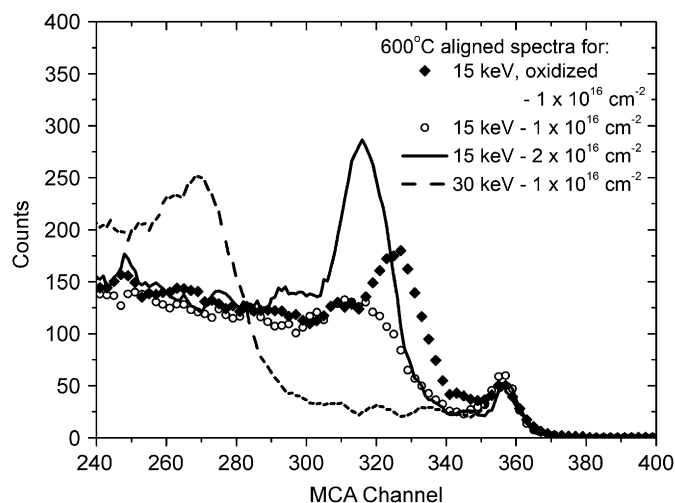


**Fig. 2.** Channeling spectra after 600 °C RTA annealing (120 s) for samples with different implantation energies: 15 keV through a 50 nm  $\text{SiO}_2$  cap (full diamond), 15 keV (open circles), and 30 keV (dashed line). All samples were implanted with  $1 \times 10^{16} \text{ He/cm}^2$ . The spectrum from the sample implanted with 15 keV up to the fluence of  $2 \times 10^{16} \text{ He/cm}^2$  is shown as the solid line.

and the small distortion in the crystal since channeling effect is very sensitive to crystal imperfections [13].

Fig. 1 shows the spectra from the sample implanted with 15 keV He ions and a fluence of  $2 \times 10^{16} \text{ He/cm}^2$ , annealed at five different temperatures in the range of 350–1000 °C. For comparison, a spectrum obtained in a non-aligned condition is also shown. Each aligned spectrum shows a small peak observed about the MCA number 360, which is due to scattering from Si atoms at the sample surface. The surface peak is characteristic in channelled spectra and corresponds to the outermost atoms seen by the beam. However, at lower MCA channel numbers a well-pronounced peak is observed (except in the 1000 °C spectrum). Our calculations, based on a surface energy approximation [13] and an estimation of stopping powers for a random target [15], show that the peak position corresponds to beam scattering from a depth of approximately 130 nm, indicating the formation of He bubbles at this depth due to annealing.

Our results show that bubbles start to form at the low annealing temperature of 350 °C (open triangles). The maximum dechanneling is already obtained after annealing at 450 °C (open circles) and stays unchanged up to about 600 °C (full diamonds). This would be consistent with the thermal behavior associated with a bubble coalescence regime, where they increase in size leading to a smaller crystal distortion. At 750 °C (dashed lines) a smaller dechanneling is observed, indicating bubble dissolution and annihilation. At the highest annealing temperature (1000 °C—solid line), the He-implanted Si completely recovers its original crystalline quality and the spectrum shows the lowest counts for all depths. These results provide the evidence that He bubbles are formed in Si(111) at a low temperature (450–600 °C). It was concluded that the growth temperature needs to be kept at around 600 °C in order to use the advantage of the stress field around the bubbles to attract the interfacial dislocations. We also showed that the duration of annealing at a particular temperature does not change the spectra, indicating the growth temperature is the main parameter. We also observed that deeper implantation obtained at 30 keV implantation energy is more thermally stable against bubble annihilation, probably due to the longer distance required for He atom to diffuse to the sample surface.

Fig. 2 shows the spectra obtained from the sample annealed at 600 °C in order to observe the change with implantation energy and fluence. When the implantation energy changes from 15 to 30 keV, the He dechanneling peak shifts from the MCA channel 315 to 268, respectively. For the 15 keV implantation through a 50 nm SiO<sub>2</sub> cap the peak is at about channel 326 (full diamond), while for the non-capped samples (open circles— $1 \times 10^{16}$  He/cm<sup>2</sup> or solid line— $2 \times 10^{16}$  He/cm<sup>2</sup>) the MCA channel is at about 315. These peak positions correspond to depths of the He bubbles of about 90, 130 and 270 nm from the sample surface, respectively. It will be shown later that these estimated values agree fairly well with those observed experimentally by TEM. One should notice a higher dechanneling peak for the 30 keV (dashed line), as compared to the 15 keV with the same fluence (open circles— $1 \times 10^{16}$  cm<sup>-2</sup>). This might indicate that the sample with bubbles located farther from the surface retained more implanted He, indicating lower out-diffusion. However, when the 15 keV oxidized sample (full diamond) is compared with the 15 keV un-oxidized one (open circles— $1 \times 10^{16}$  cm<sup>-2</sup>), the indication is that the shallowest implantation has retained more He. This can be explained by the fact that the SiO<sub>2</sub> cap also reduces the He out-diffusion during the implantation. Fig. 2 also indicates that dechanneling is increasing with the implantation fluence and the highest dechanneling peak is observed for 15 keV up to a fluence of  $2 \times 10^{16}$  cm<sup>-2</sup> (solid line).

These results demonstrate that the bubble stress field on the sample surface can be tailored by changing the implantation conditions and we can tailor the bubble stress field over the Si surface.

#### 4. Growth procedure

We explored two different growth procedures: MOCVD and molecular beam epitaxy (MBE). When MOCVD was used for the growth of GaN/AlN/Si layers, Si substrates were first cleaned in acetone, followed by methanol, DI water, and aqua regia before loading to the growth chamber (called here cleaning procedure I). Hydrogen annealing was performed for 3 min at 1020 °C. An AlN buffer layer was grown at 550 °C for 30 min, followed by annealing at 1010 °C for 5 min. After this procedure the growth of GaN at 1005 °C under 200 Torr was used, followed by growth at 1010 °C at 76 Torr. The total thickness of GaN was estimated to be ~1 μm. SEM images showed pinholes on the sample surface due to

incompleted surface coalescence due in part to small film thickness.

We also used similarly cleaned samples for the growth using an SVT MBE system having rf nitrogen plasma as the nitrogen source. One infinite cell and two add-on cells were used for the Ga and Al sources, respectively. The AlN buffer layer was grown at a temperature slightly above 600 °C, followed by the growth of GaN at a temperature 50 °C higher than the buffer layer. We also grew slightly thicker AlN layers and GaN/AlN on un-implanted and implanted <111>, Si substrates using cleaning procedure I.

Usually an annealing process at high temperature (above 1000 °C) is used to remove the surface oxide and obtain  $7 \times 7$  surface reconstruction for clean Si before the growth, but RBS results suggest using growth temperature as close as possible to 600 °C and not exceeding 750 °C. Therefore, we also explored a different cleaning procedure (II) and used an RCA wet chemical cleaning process followed by dipping of Si samples in diluted HF solution and immediately loading into the MBE system. The same N, Ga and Al sources were used. There was no additional high-temperature thermal treatment [16] of the Si substrates before the growth. To achieve a uniform temperature distribution, the wafers were supported only by thin Mo wires to avoid any hard thermal contact between the substrate and the Mo holder. The AlN buffer layer was grown at the same temperature followed by growth of GaN at a temperature 20 °C higher than in previous MBE growth. The GaN layers were grown under the Ga-rich condition and the growth rate was limited by the nitrogen flux. During the growth, reflection high-energy electron diffraction (RHEED) was used to monitor the surface condition.

#### 5. TEM studies

Characterization of GaN grown on implanted and un-implanted Si substrates was performed by TEM using a JEOL 3010 transmission electron microscope. Since the MOCVD method is most commonly used for growth of GaN, we tried to explore this possibility by using AlN as buffer layer in order to prevent Ga–Si reaction. We used a Si substrate implanted with a fluence of  $1 \times 10^{16}$  He/cm<sup>2</sup>. Before growth, wafers were cleaned using procedure I, and a short anneal at 1020 °C. A row of He bubbles was observed at 120 nm from the interface, in good agreement with the RBS channeling measurements. The diameter of the bubbles was about 40–50 nm on average. Many large elongated bubbles (100 nm and longer) were also found at the interface (Fig. 3), suggesting that the Si surface treatment at high temperature can lead to a coalescence of the bubbles and their diffusion to the sample surface. This row of bubbles was formed most probably during this 3 min annealing at 1020 °C, since no interaction with misfit dislocations was observed. The density of dislocations formed in the GaN layer grown on implanted Si was  $2 \times 10^9$  cm<sup>-2</sup>. This defect density was compared to that observed in GaN samples grown on un-implanted Si using the same cleaning and growth procedure (Fig. 4). The estimated density of dislocations in the sample grown on un-implanted Si was  $3 \times 10^9$  cm<sup>-2</sup> and was only slightly higher (probably within measurement error) than on implanted substrates. We concluded that a high annealing temperature before the growth leads to a conglomeration of He bubbles and He diffusion to the Si surface, therefore not helping so much in stress relaxation during the growth of nitrides.

Since the RBS results shown in Figs. 1 and 2 suggest highest dechanneling at 600 °C, and decreasing (but still observable) at 750 °C, we used the MBE growth method instead of MOCVD, since the lower growth temperature can be more easily applied. We were aware that the quality of the layer can suffer due to

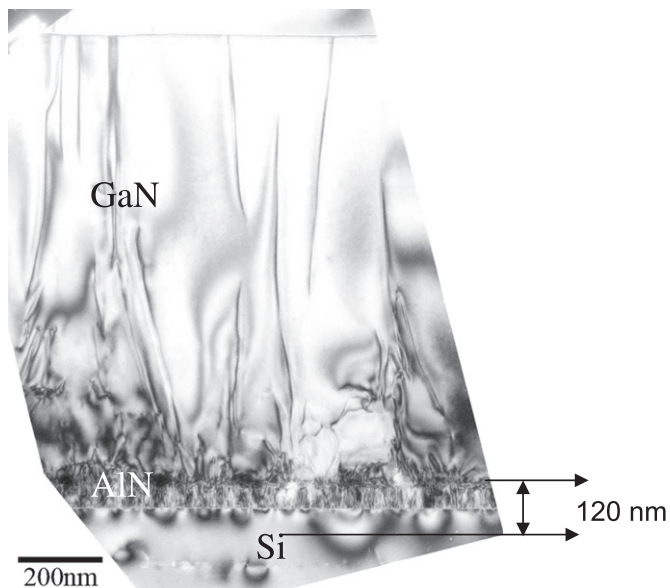


**Fig. 3.** Cross-section TEM micrograph showing He bubble formation in the implanted Si substrate ( $1 \times 10^{16}$  He/cm $^2$ ) after short annealing at 1020 °C and later growth of GaN/AlN. The estimated density of dislocations in this sample was  $2 \times 10^9$  cm $^{-2}$ .

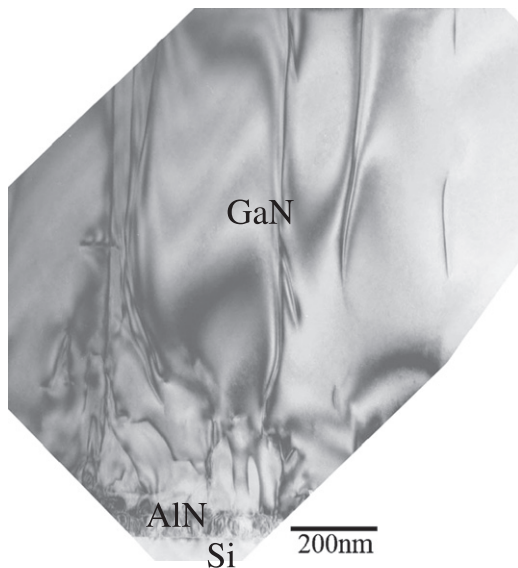


**Fig. 4.** Cross-section TEM micrograph showing dislocations formed in GaN/AlN grown on an un-implanted Si substrate. Surface treatment and growth conditions of the GaN/AlN were similar to those used in the implanted samples. Estimated density of dislocations was  $3 \times 10^9$  cm $^{-2}$ .

utilization of a low growth temperature, but the aim of these studies was to see if redirecting misfit dislocations from the interface to the substrate is possible. AlN layers were grown slightly above 600 °C with a thickness of  $\sim 30$  nm, followed by a 1  $\mu$ m thick GaN layer grown at 50 °C higher temperature than used for the buffer layer. Si wafers were cleaned by the same procedure I, as used for the MOCVD growth. However, annealing of the substrates prior to growth was not used. Samples with two different implantation energies (15 and 30 keV) and same fluence ( $1 \times 10^{16}$  He/cm $^2$ ) were studied. In addition, the same structures were grown on un-implanted Si using the same growth and substrate-cleaning procedure.

The first GaN layer  $\sim 1030$  nm thick was grown on 30–40 nm thick AlN on top of an implanted (15 keV and fluence  $1 \times 10^{16}$

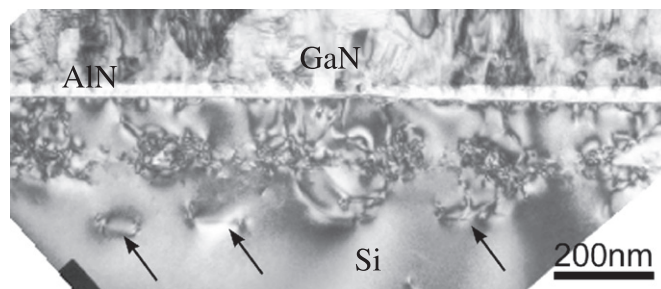


**Fig. 5.** Cross-section TEM micrograph of GaN/AlN grown on He-implanted Si (15 keV and fluence of  $1 \times 10^{16}$  cm $^{-2}$ ; He bubbles  $\sim 120$  nm from the interface). An interaction of misfit dislocations with the strain field (and possible dislocation loops) formed around the He bubbles is visible. End-of-range defects are indicated by arrows.

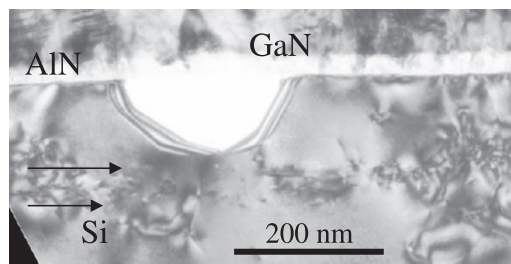


**Fig. 6.** Higher magnification of an area close to a void formed at the interface. Note the lack of misfit dislocation interaction in the area of the large void. Arrows outline a band of He bubbles.

cm $^{-2}$ ) Si substrate (Fig. 5). The measured distance from the interface to the He bubbles, based on TEM micrographs, was 120 nm, close to the nominal value of 130 nm determined by RBS. In this sample misfit dislocations interacted with the strain field created around many He bubbles and these dislocations propagated further into the substrate. There are, however, some He bubbles around which this action did not take place. It was noticed that the distance between the redirected dislocations (50–200 nm) propagating to the substrate was many times larger than the expected distance between misfit dislocations at the AlN/Si interface ( $\sim 15$ – $20$  Å) and diameter of the bubbles. The bubbles have a diameter close to 15 nm, the distance between the bubble perimeters was about 20 nm (about 25 nm from center to center) and they formed in a thin 50–60 nm band. Therefore, if the mechanism described earlier [11] applies, then more misfit dislocations should be attracted to the He bubbles. Further studies are needed to understand this observation. End-of-range defects in the form of dislocation loops formed due to implantation were also clearly observed. There are also some areas of the samples where large voids are formed at the interface (Fig. 6). Any interaction with dislocation loops in the vicinity of such a void was not observed.

A higher implantation energy (30 keV) and fluence ( $1 \times 10^{16}$  cm $^{-2}$ ) (Fig. 7) was also studied. The GaN layer ( $\sim 1050$  nm thick) was grown on 40 nm thick AlN on top of an implanted Si substrate. The distance from the interface to the He bubbles in this case was  $\sim 240$  nm, close to the nominal value of 270 nm. Only a narrow band with He bubbles was observed in this area of the Si substrate. In this sample some misfit dislocations interacted with the strain field around the bubbles and propagated deep to the substrate where end-of-range defects are formed and beyond. However, the distance between the dislocations that propagated from the interface to the Si substrate was much larger (200–400 nm) than in the sample with a lower fluence and shorter distance from the Si surface. It is most likely that the He

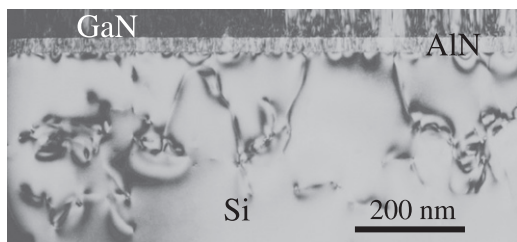


**Fig. 7.** Cross-section micrograph from the GaN/AlN layers grown on implanted Si substrate (30 keV and fluence of  $1 \times 10^{16} \text{ cm}^{-2}$ ) showing misfit dislocations redirected into the Si substrate. Some dislocations propagated farther into the Si substrate (beyond the end-of-range defects).

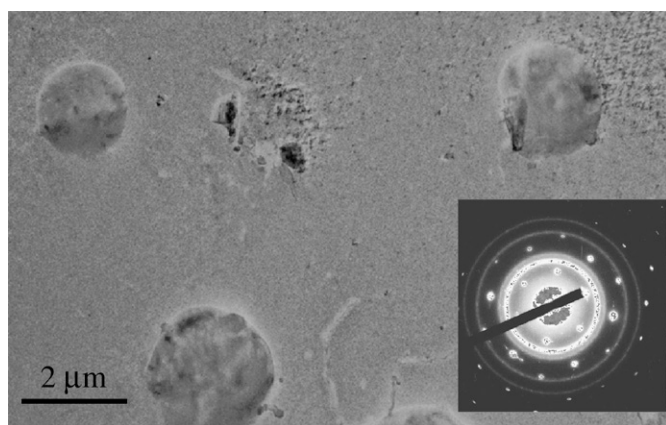


**Fig. 8.** A plan-view micrograph from the AlN layer (80 nm thick) grown on top of an un-implanted Si substrate. Note the large islands imbedded into the AlN layer. The ring diffraction pattern (inset) indicates the polycrystalline nature of the AlN layer superimposed with a spot diffraction pattern from the Si substrate.

bubbles are formed too deep in the substrate and the strain field around them is not large enough to interact with misfit dislocations formed at the interface with the AlN buffer layer. Dislocation density in the GaN layer was rather large ( $9 \times 10^{11} \text{ cm}^{-2}$ ).

Samples that were implanted (15 keV and fluence of  $1 \times 10^{16} \text{ cm}^{-2}$ ) through the  $\text{SiO}_2$  cap layers (removed before the growth), where He bubbles are formed at the depth of 70 nm, did not show strong interaction with the misfit dislocations since many elongated voids were present at the interface with the AlN buffer layer. From these studies it was clear that there is only a narrow range of distances at which interaction with misfit dislocations is possible. It was also observed that despite many misfit dislocations being “pushed” back to the Si substrate the GaN layer quality did not improve. It was clear that this low growth temperature was one of the parameters determining the GaN quality. The second parameter that we also considered was a cleaning procedure, since the traditionally used annealing procedure for oxide removal could not be applied in this case.

To check the influence of growth temperature, we performed an experiment with the growth of a slightly thicker (80 nm) AlN layer (without GaN) since AlN is the first layer deposited on the Si substrate. Misfit dislocations formed at this AlN/Si interface interact with the strain field around He bubbles and perfection of this layer will influence the quality of GaN layer grown on top of it. We grew an AlN layer on implanted and un-implanted Si substrates, using MBE and the same cleaning procedure and growth temperature as used previously. Cross-section and plan-view samples have been studied. A large strain at the interface causing sample bending and rather poor AlN structural quality is

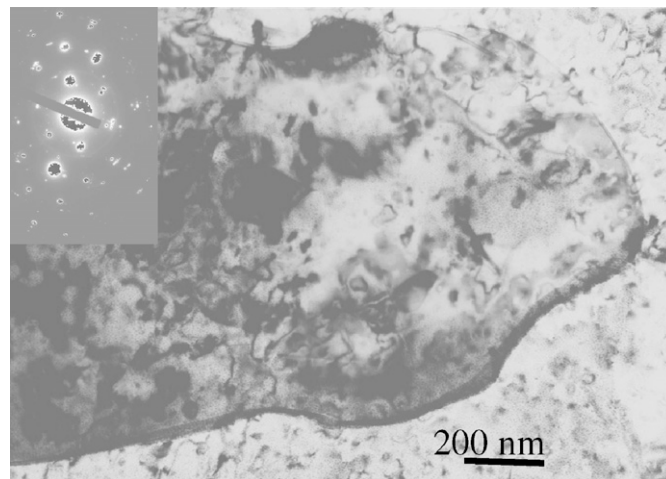


**Fig. 9.** The micrograph of the island in larger magnification. Note that this island is more crystalline than the surrounding area. Separate elongated spots from the AlN are visible in the diffraction pattern (inset).

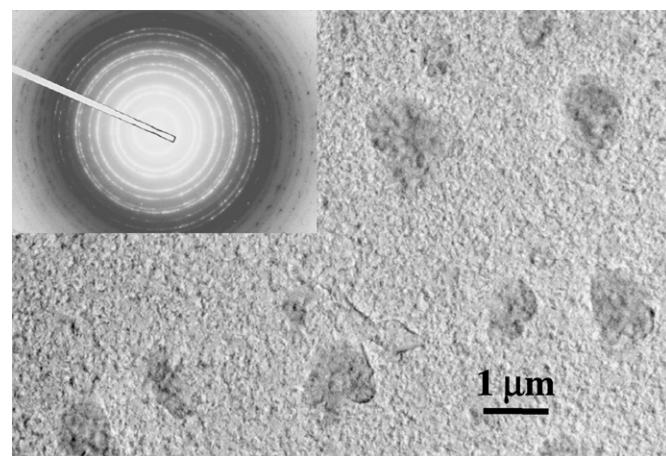


**Fig. 10.** A plan-view micrograph from the wafer center of the 80 nm thick AlN layer grown on top of the He-implanted (15 keV and fluence of  $1 \times 10^{16} \text{ cm}^{-2}$ ) Si substrate. Note the islands  $\sim 1 \mu\text{m}$  in diameter imbedded into the layer. A ring diffraction pattern (inset) indicates the polycrystalline nature of this sample.

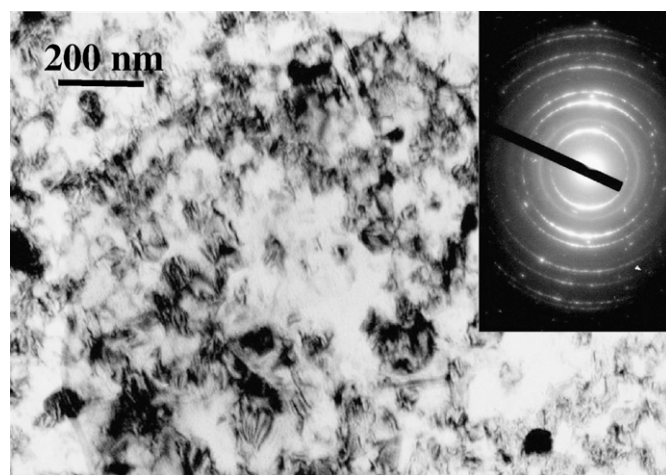


**Fig. 11.** Larger magnification of the center part of the island. An inset shows arcing diffraction rings suggesting that the sample is textured.

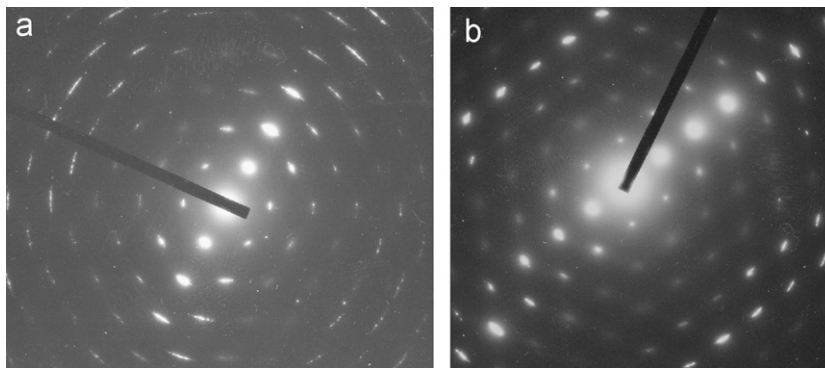


**Fig. 12.** Electron diffraction patterns from GaN grown on un-implanted (a) and implanted (b) Si substrate cleaned using procedure II ( $1 \times 10^{16} \text{ cm}^{-2} \text{ He}$ ).

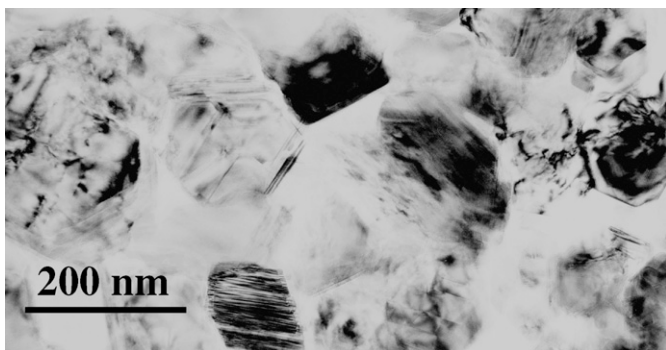


**Fig. 13.** Plan-view micrograph from the GaN layer grown on unimplanted Si (with AlN buffer layer) taken with multi-beam conditions to observe all grains in contrast.

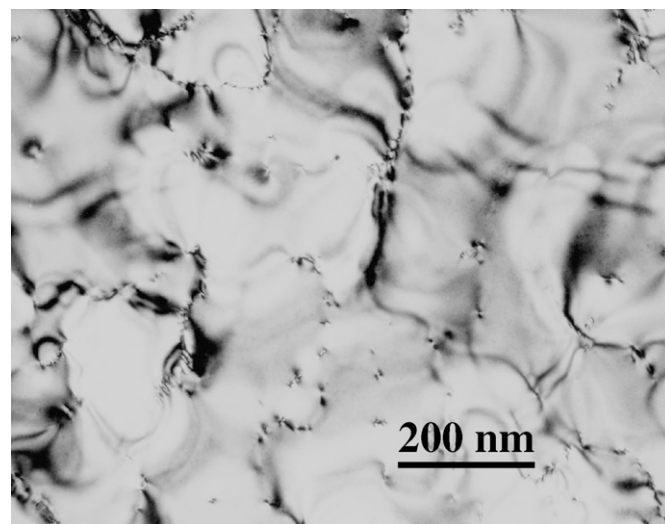


**Fig. 14.** Plan-view micrograph from the GaN grown on He-implanted ( $1 \times 10^{16} \text{ cm}^{-2}$ ) Si substrates (with AlN buffer layer) showing large grain diameter. The subgrain diameter (with dislocations on grain boundaries) is more than 1000 nm. Growth conditions and cleaning procedure II were kept identical as for the growth on un-implanted Si.

observed for the layers grown on the un-implanted substrate. In plan-view images (Fig. 8) large islands (with a larger thickness) were imbedded in the layer with a smaller thickness. The diffraction pattern (Fig. 8) is a superposition of a ring pattern from AlN and spot pattern from the Si substrate. Larger islands also show polycrystalline nature (Fig. 9), with a similar ring diffraction pattern superimposed with Si spot pattern.

For the AlN layer grown on implanted substrates, plan-view TEM samples also showed larger islands with higher thickness imbedded in these layers (Fig. 10). A diffraction pattern taken with a large selective area aperture shows the textured nature of this sample (Fig. 10 inset), with clear arcs on the diffraction pattern (Fig. 11 inset) suggesting slightly better quality compared to the samples grown on un-implanted substrates. Indeed, cross-section samples indicate more relaxation at this interface. The quality of this layer was, however, not satisfactory. Therefore, we changed to cleaning procedure II for Si substrates.

A new set of GaN/AlN/Si samples was grown in the same MBE system. Cross-section and plan-view samples were studied by TEM. Diffraction patterns and bright field micrographs prepared from plan-view samples show a drastic difference in the structural quality of these samples. Diffraction patterns (Figs. 12a–b) show a much higher arcing of the diffraction spots from the samples grown on un-implanted Si, suggesting smaller grains and misorientation between them. This arcing is practically negligible in the samples grown on implanted substrates and single-crystal pattern is observed (Fig. 12b). This substantial improvement in the structural quality of the GaN layer is confirmed by images taken from these layers grown on the un-implanted and implanted substrates (Figs. 13 and 14). The size of the grains for the layers grown on implanted Si (Fig. 14) was many times larger (few 1000 nm) than for the growth on un-implanted Si (Fig. 13). The

size of the GaN grains for the samples grown on un-implanted Si was in the range of 40–150 nm. A large misorientation between these grains was observed. Since the lattice mismatch and difference in thermal expansion coefficient between Si and GaN (and also AlN) are so large, a complete removal of threading dislocations is practically impossible, but the quality of the GaN layers obtained by application of this growth procedure is remarkable and comparable to the structural perfection of GaN grown on  $\text{Al}_2\text{O}_3$ . It is believed that the quality of GaN can be further improved by optimization of the growth and surface-cleaning procedures.

## 6. Summary

For the first time, it has been shown that misfit dislocations formed at the GaN/AlN/Si interface can interact with a strain field formed around He bubbles created in He-implanted Si which allow redirecting of the misfit dislocations into the Si substrate instead of the epi-layer. It was found that an implantation dose of ( $1 \times 10^{16} \text{ cm}^{-2}$ ) at 15 keV, which forms He bubbles 120 nm from the interface, gives the best results. Too small or too large distance of the bubbles from the interface does not lead to the interaction with misfit dislocations formed during the growth of the AlN buffer layer. If voids are created at the interface, then an

interaction with misfit dislocations does not take place. Placement of bubbles further from the interface at 240 nm (keeping the same implantation dose) still works, but the density of redirected dislocations is smaller. This study also showed that in order to form He bubbles a low growth temperature for the AlN layer is required. Pretreatment of the Si surface in order to get a  $7 \times 7$  reconstruction (proof of a clean surface) cannot be used because He bubbles diffuse to the interface and do not produce a strain field dislocation loops around them to attract interfacial dislocations.

This study also shows that in order to improve structural quality (in addition to redirecting the dislocations to the substrate) the proper cleaning procedure of the Si substrate and a well-defined growth temperature (a temperature at which He bubbles do not propagate to the substrate surface) needs to be applied. Our recent results show remarkable structural quality of GaN grown on He-implanted Si. There are no cracks and grain diameter is comparable to the one observed for samples grown on  $\text{Al}_2\text{O}_3$ , despite the large lattice mismatch and differences in thermal expansion coefficient (not present for growth on sapphire). Further development of this method may make a combination of sophisticated Si technology with the strength of GaN a reality.

### Acknowledgments

This work was financially supported by the Air Force Office of Scientific Research under order No. OGMORD 52K44134. Use of the facility in the National Center for Electron Microscopy in LBNL, Berkeley, CA is greatly appreciated. J. Xie and H. Morkoç would

like to thank Dr. R.J. Malik from RJM Semiconductor for the development of the Infinite Ga cells for the MBE system.

### References

- [1] A. Dadgar, F. Schulze, M. Wienecke, A. Gadanez, J. Blasing, P. Veit, T. Hempel, A. Diez, J. Christen, A. Krost, N. J. Phys. 9 (2007) 387.
- [2] A. Dadgar, M. Poschenrieder, J. Blasing, O. Contreras, F. Bertman, T. Riemann, A. Reiher, M. Kunze, I. Daumiller, A. Krtschil, A. Diez, A. Kaluza, A. Modlich, M. Kamp, J. Christe, F.A. Ponce, E. Kohn, A. Krost, J. Crystal Growth 248 (2003) 556.
- [3] A. Krost, A. Dadgar, F. Schulze, J. Blasing, G. Strasburger, R. Clos, A. Diez, P. Veit, T. Hempel, J. Christen, J. Crystal Growth 275 (2005) 209.
- [4] S. Fang, K. Adomi, S. Iyer, H. Morkoç, H. Zabel, C. Choi, N. Otsuka, J. Appl. Phys. Rev. 68 (1990) R31.
- [5] A. Sakai, H. Sunakawa, A. Usui, Appl. Phys. Lett. 71 (1997) 2259.
- [6] Z. Liliental-Weber, M. Benamara, W. Swider, J. Washburn, J. Park, P.A. Grudowski, C.J. Eiting, R.D. Dupuis, MRS Internet J. Nitride Semicond. Res. 4S1 (1998) G46.
- [7] Z. Liliental-Weber, D. Cherns, J. Appl. Phys. 89 (2001) 7833.
- [8] T. Zheleva, S. Smith, D. Thomson, K. Linthicum, P. Rajagopal, R.F. Davis, J. Electron. Mater. 28 (4) (1999) L5.
- [9] P. Fini, H. Marchand, J.P. Ibbetson, B. Moran, L. Zhao, S.P. Denbaars, J.S. Speck, U. Mishra, Mater. Res. Soc. Symp. Proc. 572 (1999) 315.
- [10] R.F. Davis, T. Gehrke, K.J. Linthicum, T.S. Zheleva, E.A. Preble, P. Rajagopal, C.A. Zorman, M. Mehregan, J. Crystal Growth 225 (2001) 134.
- [11] H. Trinkaus, B. Holander, St. Rongen, S. Mantl, H.J. Herzog, J. Kuchenbeckern, T. Hackbarth, Appl. Phys. Lett. 76 (2000) 3552.
- [12] M. Luysberg, D. Kirch, H. Trnkaus, B. Hollander, St. Lenk, S. Mantl, H.J. Hertzog, T. Hackbarth, P.F.P. Fichtner, J. Appl. Phys. 92 (2002) 4290.
- [13] Wei-Kan Chu, James Mayer, Marc-A. Nicolet, Backscattering Spectrometry, Academic Press, New York, 1978.
- [14] P.F.P. Fichtner, et al., Nucl. Instrum. Methods B 136–138 (1998) 460.
- [15] J.F. Ziegler, J.P. Biersack, U. Littmark, The Stopping and Range of Ions in Solids, Vol. 1, Pergamon Press, Oxford, 1985.
- [16] F. Semond, B. Damilano, S. Vezian, N. Grandjean, M. Lerous, J. Massies, Appl. Phys. Lett. 72 (1992) 82.